Hardial Singh* and B.B. Arora

Effects of casing angle on the performance of parallel hub axial annular diffuser

https://doi.org/10.1515/tjj-2020-0019
Received June 23, 2020; accepted June 29, 2020; published online August 17, 2020

Abstract: In this paper, the effects of non-swirling and swirling flow on the performance of parallel hub axial annular diffuser has been investigated. The study was conducted on a fully developed swirling flow and non-swirling flow to predict the separation of the flow from the wall. Three different annular diffusers were used with casing wall angles of 3°, 6°, and 9°. Furthermore, various swirl angles (0–25°) at the inlet of diffusers have been investigated to analyze the performance across the length. It was found that parallel hub axial annular diffuser performance increases up to a certain length as the inlet swirl angle increases. However, the performance also improves as the diffuser area ratio (AR) increases. The performance is evaluated based on the static pressure recovery coefficient (C_p) and the total pressure loss coefficient (C_{TL}). The highest possible pressure recovery is achieved by the 12° swirl angle with a casing angle of 6°.

Keywords: annular diffuser; inlet swirl; static pressure recovery coefficient; total pressure loss coefficient.

PACS2010 classification: (47.11.-j Computational methods in fluid dynamics).

Introduction

Annular diffusers are extensively used in engineering applications such as outlet devices in case of the pump, turbines located in downstream turbomachinery, and in other numeral applications. In aircraft applications, an annular diffuser commonly operates at the downside of the compressor. The annular diffuser operates in the presence of swirl flow in turbomachinery. The swirl flow is generated by guide vanes located at the inlet and by some other components such as strut and by revolving of the central shaft passing through the diffuser and the compressor. The improvement in the overall performance of the system is due to a change in flow velocity caused by the swirl effect [1–2]. Swirling flow through diffuser was investigated by many researchers to analyze the behavior of the flow. Singh and Arora [3] carried out the work on annular diffuser having cone angle 20°, and AR varying between 2 and 4. The results show that maximum performance was achieved with swirl flow on the AR 2. Johnston [4] worked on annular diffusers having an AR of 3.2 and divergence angle varying from 6.5° to 15°. The performance of diffusers decreases as the divergence angle increases. Reneau et al. [5] performed the work on a series of two-dimensional diffusers and found that $6° \le 2\theta \le 8°$ gave the highest pressure recovery at a constant area ratio (AR). The efficiency of diffusers decreases as the divergence angle increases. Sovran and Klomp [6] studied more than one hundred geometries with conically central diverging center bodies having a radius ratio of 0.5–0.70. The test was conducted on the thin boundary layer fluid flow with free discharge and it was observed that the diffuser effectiveness decreases as the blockage increases for two dimensional flow. Stevens [7]; Adenubi [8] reported that there was a boost of 10–12% in the pressure recovery results when the turbulence intensity in annular diffuser increases from 4 to 10%. Critically distorted asymmetric inlet velocity profiles produce a severe drop in pressure recovery. Stevens and Fry [9] worked on two optimum straight-walled annular diffusers. One diffuser had a uniform diameter center body, the other had an expanding diameter center body (divergence angle 40°). Measurements of the pressure recovery, loss of total pressure, velocity profile in terms of boundary layer growth, and turbulence level were taken. Coladipietro et al. [10] reported that in the short diffusers, the variation of pressure recovery with blockage was similar to the channel and conical diffusers. The findings show that pressure recovery decreases with increasing blockage. Kumar and Kumar [11] concluded the swirling flow on the subsonic turbulence in the diverging equal hub and casing boundaries of annular diffusers. An inlet swirl reduces the flow separation that occurs at the casing of a stalled diffuser. Further, a large inlet swirl may result in the removal of the stall from the casing to the hub.

***Corresponding author: Hardial Singh**, Department of Mechanical Engineering, Delhi Technological University, Delhi, 110042, India, E-mail: hardialsingh3@gmail.com
B.B. Arora, Department of Mechanical Engineering, Delhi Technological University, Delhi, 110042, India, E-mail: bbarora@dce.ac.in

Singh et al. [12]; Singh et al. [13] showed the improvement in the performance of annular diffuser by using swirl flow in their experimental data. It is found that flow separation occurs on the hub wall and diminishes the performance beyond the swirl angle 30°. Mohan et al. [14] examined three annular diffusers with AR 3 and a half cone angles of 12.5°, 15°, and 17.5°. In each of the diffusers, the 6–8 level of swirl has been imparted at the inlet. It was deduced that the inlet swirls up to a particular level to improve the pressure recoveries but after that has a detrimental effect. Maximum pressure recoveries obtained were 72, 69, and 66% for the 12.5°, 15°, and 17.5° cases, respectively. Ubertini and Desideri [15]; Feldcamp and Birk [16] analyzed the performance of annular diffuser experimentally with and without strut. It was observed that performance improves with strut for the stalled diffuser. In the no swirl condition, there is a small effect of total pressure loss with the presence of strut. The pressure recovery assisted by the strut with an increase in swirl angle by 20°.

Literature shows that in addition to dynamic parameters such as velocity profile at inlet, inlet Reynolds number, and swirl flow at the inlet the performance of the axial annular diffuser also depends on the geometric parameters such as length L, AR, hub wall angle, and casing wall angle. The present analysis has been conducted for a constant axial length (L = 33.76 cm) with casing wall angles (3°, 6°, 9°) and (AR = 1.67, 2.48, 3.44) for the parallel hub axial annular diffuser. The performance characteristics of the diffuser have been evaluated based on non-swirling flow (0°) and swirl flow (7.5°, 12°, 17°, 25°) at the inlet. The computational study has been carried out on three different two-dimensional axisymmetric diffusers. The velocity profile obtained from the experiment was introduced in ANSYS Fluent with dynamic parameters in different turbulence models for swirling and non-swirling flow. The turbulence model, which is prognosticating the result more closely with the experimental results, was chosen for further investigation. The geometrical parameters of the annular diffuser are shown in Table 1 and Figure 1.

Table 1: Geometrical parameter of the annular diffuser.

R_{hi} = 38 mm R_{ci} = 77.5 mm, R_{ho} = 38 mm, $(R_h/R_c)_i$ = 0.49, L/ΔR = 8.54, θ_h = 0°, L = 33.76 cm			
Types of diffuser	**θ_c**	**R_{co}(cm)**	**AR**
A	3°	9.52	1.67
B	6°	11.3	2.48
C	9°	13.1	3.44

Experiment test rig

The experimental test rig consists of a centrifugal blower, a conical diverging section, a settling chamber, a swirl plate, an annulus cross-sectional area, and an annular diffuser as shown in Figure 2. The centrifugal blower delivers air at a flow rate of 1.5 m^3/s and at a pressure equal to 0.1 bar. The air drawn from the ambiance is delivered to the conical diverging cross-sectional area which is then passed to the settling chamber having a honeycomb cross-section and very fine mesh screen. A flexible coupling of heavy fabric placed between the settling chamber and the blower avoids the vibration from reaching the blower to the settling chamber. The settling chamber consists of multiple folds of screen for decreasing the turbulence level, and for damping the flow fluctuations. The uniform flow enters into a constant area annular pipe from the smooth converging cross-section. A swirl plate with 12 vanes is installed at the entry of the annular passage to achieve the desired swirl level. The swirl plate is mounted at the upstream of the test diffuser to avoid the vane wake entry into the diffuser and also for the recovery of pressure, which is lost across the plate. The casing wall of the test diffuser is manufactured from Perspex. There are number of static pressure taps on the casing wall and hub wall along the length of the test diffuser for the measurement of static pressure using manometers. The longitudinal and swirl velocities are measured with a cobra probe. The null technique is used along the different axial locations in the test diffuser. The cobra probe yaw angle is set to zero by aligning with the incoming flow in this technique. The calibration range associated with the cobra probe is to measure the velocity within ±55°. The uncertainty of the manometer for measurement of the static pressure is ±1.5 mm of water, and the total pressure is ±1 mm of water.

Computational domain and boundary condition

The axisymmetric two-dimensional geometry of the annular diffuser has been modeled in the ANSYS workbench with proper dimensions, as shown in Figure 3. A mapped meshing scheme has been used on the computational domain with quadrilateral elements for all the cases. The mesh quality is controlled by maintaining the aspect ratio (less than 50) and skewness in the geometry. The distance of the first element from the wall is 0.03 mm as per y + <1. The boundary condition fed at the inlet in ANSYS Fluent is the velocity profile obtained from the experimental set up with a 3% turbulence level in the turbulence specification and the hydraulic diameter (h_d)

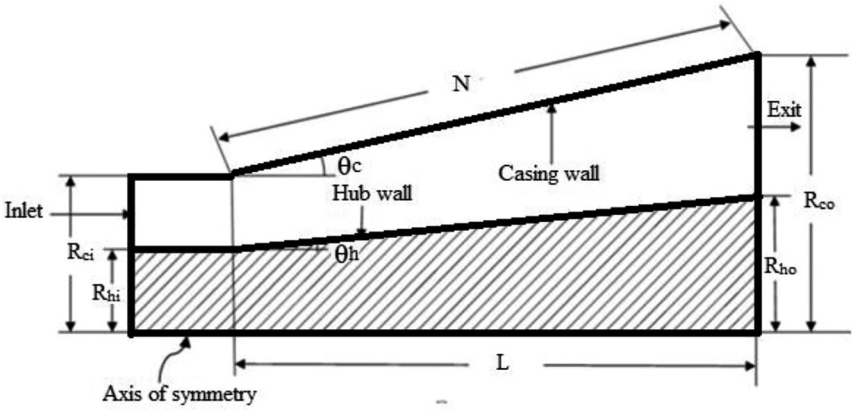

Figure 1: Diffuser geometrical parameters.

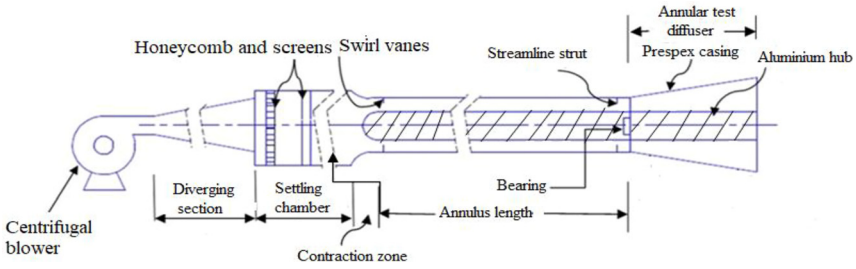

Figure 2: Experimental test rig.

value is as per the inlet geometry of diffuser. The boundary conditions are normal pressure, 3% level of turbulence, and hydraulic diameter (h_d) at the diffuser outlet. For better accuracy of the results, the 2nd order upwind scheme was used to control the solution for momentum, swirl velocity, turbulent kinetic energy (k), and turbulent dissipation rate (ω). The residuals convergence criterion of 10^{-6} was employed to achieve convergence with an SIMPLE algorithm.

Governing equations

The continuity equation of 2D axisymmetric geometry is given by

$$\frac{\partial}{\partial x}(\rho v_x) + \frac{\partial}{\partial x}(\rho v_r) + \frac{\rho v_r}{r} = s_m \tag{1}$$

Here x, and r represent the axial and radial coordinate, respectively. υ_x, and υ_r represent the axial velocity and radial velocity, respectively. s_m represents the mass added to the continuous phase from the dispersed phase.

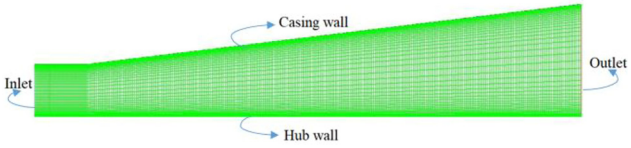

Figure 3: 2D computational domain with boundary conditions.

The governing equation for steady axisymmetric non-swirling flow, and the conservation of axial and radial momentum equation is written as

$$\frac{1}{r}\frac{\partial}{\partial x}(r\rho v_x v_x) + \frac{1}{r}\frac{\partial}{\partial r}(r\rho v_r v_x) = -\frac{\partial p}{\partial x} + \frac{1}{r}\frac{\partial}{\partial x}\left[r\mu\left(2\frac{\partial v_x}{\partial x} - \frac{2}{3}\left(\nabla.\vec{v}\right)\right)\right] + \frac{1}{r}\frac{\partial}{\partial r}\left[r\mu\left(\frac{\partial v_x}{\partial r} + \frac{\partial v_r}{\partial x}\right)\right] + F_x \tag{2}$$

and

$$\frac{1}{r}\frac{\partial}{\partial x}(r\rho v_x v_r) + \frac{1}{r}\frac{\partial}{\partial r}(r\rho v_r v_r) = -\frac{\partial p}{\partial r} + \frac{1}{r}\frac{\partial}{\partial x}\left[r\mu + \left(\frac{\partial v_r}{\partial x} + \frac{\partial v_x}{\partial r}\right) \times\right] + \frac{1}{r}\frac{\partial}{\partial r}\left[r\mu\left(2\frac{\partial v_r}{\partial r} - \frac{2}{3}\left(\nabla.\vec{v}\right)\right)\right] - 2\mu\frac{v_r}{r^2} + \frac{2}{3}\frac{\mu}{r}\left(\nabla.\vec{v}\right) + \rho\frac{v_z^2}{r} + F_r \tag{3}$$

where

$$\nabla.\vec{v} = \frac{\partial v_x}{\partial x} + \frac{\partial v_r}{\partial r} + \frac{v_r}{r} \tag{4}$$

The swirling flow needs to be solved by tangential momentum equation which can be written as

$$\frac{1}{r}\frac{\partial}{\partial x}(r\rho v_x v_z) + \frac{1}{r}\frac{\partial}{\partial r}(r\rho v_r v_z) = \frac{1}{r}\frac{\partial}{\partial x}\left[r\mu\frac{\partial v_z}{\partial x}\right] + \frac{1}{r^2}\frac{\partial}{\partial r}\left[r^3\mu\frac{\partial}{\partial r}\left(\frac{v_z}{r}\right)\right] - \rho\frac{v_r v_z}{r} \tag{5}$$

Here υ_z represents the swirl velocity

Diffuser performances

Static pressure recovery coefficient (C_p)

The magnitude of the kinetic energy of flowing fluid transforms in to pressure energy due to the diffusing action at any cross-section along the length of the annular diffuser Dunn et al. [17].

$$C_p = \frac{P_{\text{out}} - P_{\text{in}}}{0.5\rho u_{\text{avg}}^2}$$

Here

- P_{out} is the static pressure rise at the outlet;
- P_{in} is the static pressure at the inlet;
- u_{avg} is the average velocity of the fluid.

Total pressure loss coefficient (C_{TL})

It is characterized by what quantity total pressure is lost to the average inlet dynamic pressure because of viscous forces and turbulent intermixing by Buice and Eaton [18]; Ibrahim et al. [19].

$$C_{TL} = \frac{P_{\text{tin}} - P_{\text{tout}}}{0.5\rho u_{\text{avg}}^2}$$

Where P_{tin} and P_{tout} represent the total pressure at the inlet and outlet section of the diffuser, respectively.

Diffuser effectiveness (η)

It represents the ratio of real recovery of pressure diffusers to the ideal recovery of pressure diffusers for the same AR.

$$\eta = \frac{C_p}{C_{pi}}$$

$$C_{pi} = 1 - \frac{1}{AR^2}$$

Grid independence test and validation of results

The test was performed to obtain the optimal mesh size after performing the convergence study. The mesh independence test was performed on the parallel hub axial annular diffuser with AR = 2.44, casing angle 6°, and axial length 33.77 and $R_e = 2.5 \times 10^5$. Four types of mesh sizes have been tested with a turbulence model of RNG k-ε for swirl flow. Figure 4 shows the longitudinal velocity distribution profile at non-dimensional axial length (x/L) = 3 with four grid sizes having cell count (mesh 1 = 100,000 elements, mesh 2 = 160,000 elements, mesh 3 = 200,000 element, and mesh 4 = 250,000 elements). The longitudinal velocity profile for mesh 3 and mesh 4 at x/L = 0.3 are very close to each other. Hence, mesh 3 is used for the analysis of the results in the present study. The simulation was carried out using a system having i8 processor with 16 GB RAM. By using this configuration, the average time of 20 h is required for the simulation to converge. The computational results obtained from axial annular diffuser were validated with the experimental results as shown in Figure 5. The Figure presents the dimensionless velocity profile at x/L = 0.7 with different turbulence model (k-ε standard, k-ε RNG, k-ε realizable, k-ω standards, and k-ω sst) [20–21]. These models were tested against the velocity profile obtained experimentally from the axial annular diffuser at fully developed swirl flow. The k-ε RNG turbulence model shows very slight deviations from experimental results in comparison with k-ε realizable and k-ω sst. Hence RNG k-ε turbulence model is employed for further investigation for swirl flow in the axial annular diffuser with different casing angles.

Results and discussion

The flow behavior and performance of the three diffusers with different swirl flow conditions along the length have been presented and discussed in the form of the turbulence intensity, velocity vector, non-dimensional longitudinal velocity, swirl velocity, static pressure recovery coefficient (C_p), and total pressure loss coefficient (C_{TL}). The simulation was performed for five swirl conditions i.e. 0°, 7.5°, 12°, 17°, and 25° on the three diffusers. The detailed data of the analysis at 0°, 12°, and 25° inlet swirl angles are presented below.

Turbulence intensity

Figure 6 shows the turbulence intensity at the entry of diffusers with different inlet swirl angle in the annulus passage. There is a significant variation observed in the turbulence intensity from the hub to the casing wall and a strong shear layer is observed close to the casing wall. The graph shows that swirl does not affect the magnitude of intensity and

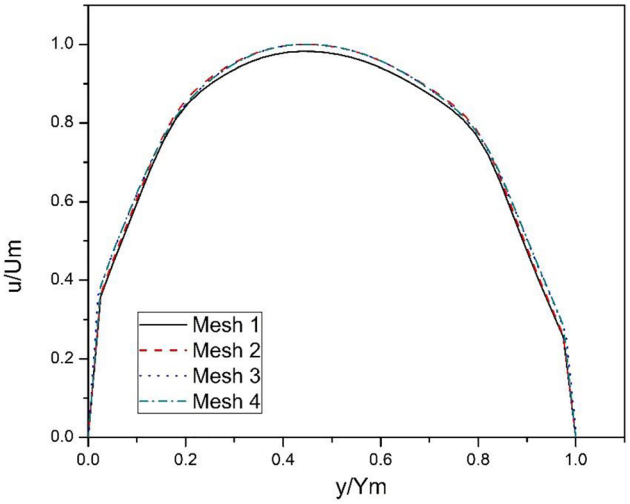

Figure 4: Longitudinal velocity profile comparison at x/L = 0.3.

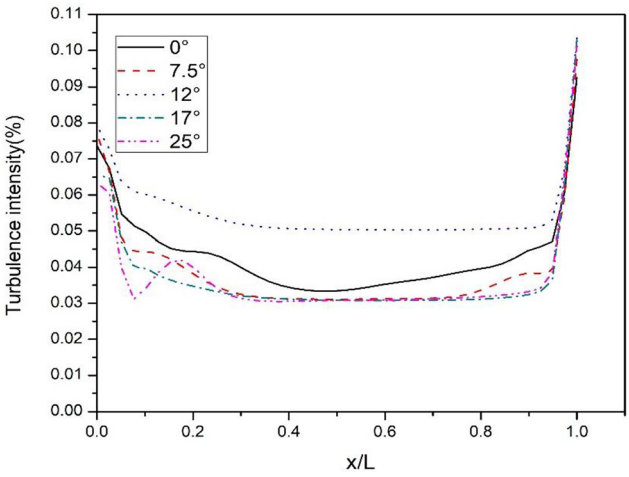

Figure 6: Turbulence intensity at the inlet.

nature of the distribution. The nature of turbulence intensity for swirl and non-swirl flow at the inlet is similar to the studies by Coladipietro et al. [10] and Hoadley [22].

Velocity vector

Figure 7(i–ix) shows the velocity vector in parallel hub axial annular axisymmetric diffuser at different inlet swirl angles 0°, 12°, and 25°. The direction of the vector clearly shows that flow is moving from the inlet to outlet of the diffuser passage with different inlet swirl angles. It is clear from Figure 7(i) that the flow is uniformly distributed between the hub and the casing wall from inlet to outlet of the diffuser passage. As the swirl angle increases up to 25°, the flow moves towards the casing wall from the hub due to less diffusion annular space, there is no turning of flow on the hub, and there exist less skin friction drag on the parallel hub as shown in Figure 7(iii). The reversal of flow occurs on the hub wall at the swirl angle 25° for B type diffuser due to the adverse pressure gradient on the wall. The reversal of flow occurs at 12°and 25° inlet swirl angles for C-type diffuser due to the high casing divergent angle and the escalation of centrifugal force take place toward the casing at high inlet swirl angle.

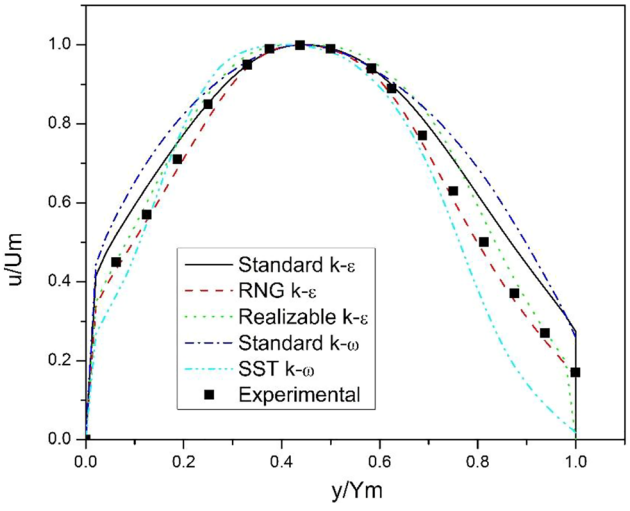

Figure 5: Validation of the turbulence model with the experimental result of the longitudinal velocity profile distribution of casing angle 6°at x/L = 0.7.

Velocity profile

All velocity profiles have been represented in the form of non-dimensional velocity at different diffuser passage, i.e., ratio of the local velocity to the local maximum velocity of the cross-section, as in Ref. [23]. The value $y/Y_m = 0$ is designated as the hub wall position of the traverse, and non-dimensional radial length $(y/Y_m) = 1$ is designated as the casing wall position. Figure 8, shows non-dimensional velocity profiles at x/L = 0.1, 0.3, 0.5, 0.7, and 0.9 of the diffuser passage for all ARs and inlet swirl angles. If the swirl is absent, the bulk flow is only between the hub and the casing wall. By introducing swirl at the inlet, the flow moves from the hub to the casing wall. There is no separation, and the reversal of flow occurs at any swirl angle for AR = 1.67 and for casing divergence angle 3° of A-type diffuser. The peak of the longitudinal velocity shift occurs towards the casing in the order of x/L = 0.9 with swirl angles 12° and 25° at $y/Y_m = 0.49$ and 0.71 for A-type diffuser. The swirl velocity distribution corresponding to the inlet swirl angles 12° and 25° are shown in Figures 8(iii) and 9(ii) respectively. It can be seen that

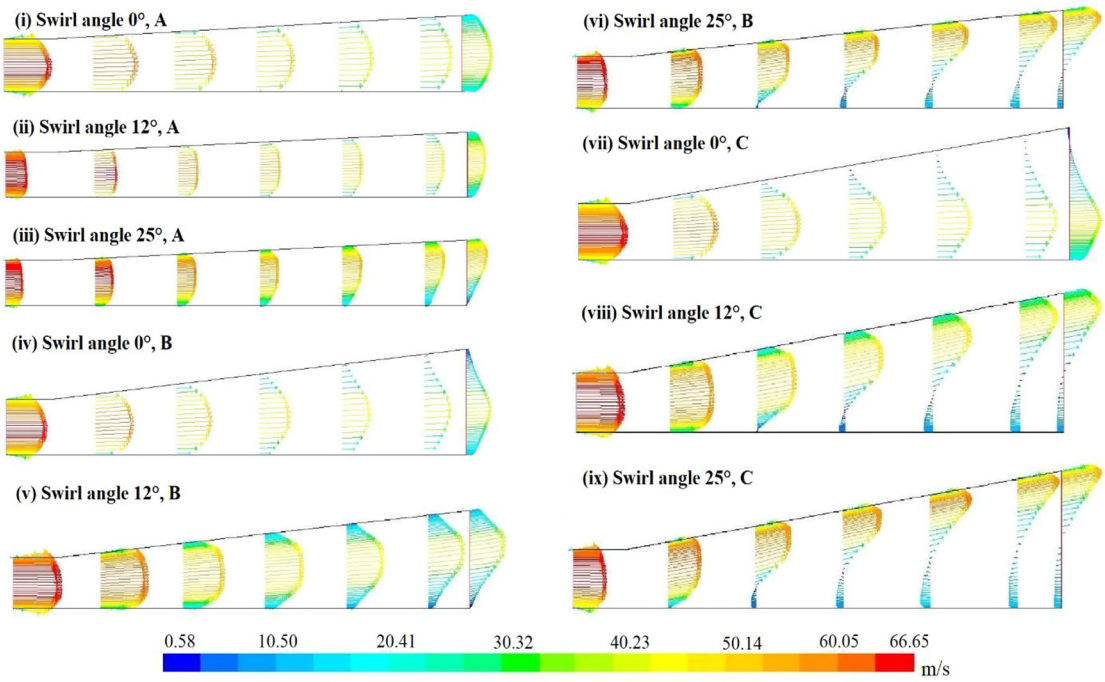

Figure 7: Velocity vector contours at swirl angles 0° (i, iv, vii), 12° (ii, v, viii) and 25° (iii, vi, ix) of diffusers A, B, and C.

continuous diffusion takes place along the diffuser length, and the high diffusing phenomenon occurs closer to the casing wall. The trends are the same in swirl velocity profile for all the cases but differ in magnitude as seen in Figures 8(iii) and 9(ii).

The longitudinal velocity distribution profiles in the straight hub of the B-type diffuser with casing divergence angle 6°, AR = 2.48 are shown in Figures 10(i, ii) and 11(i). For no swirl condition, the flow shifts to the hub wall while with the swirl flow it shifts to the casing wall. The high diffusing phenomenon occurs due to the large casing angle and availability of more annular space. The maximum velocity at x/L = 0.9 in the AR of 2.48 observed at y/Y_m = 0.56, 0.87 for swirl angle 12°, and 25° in a B type

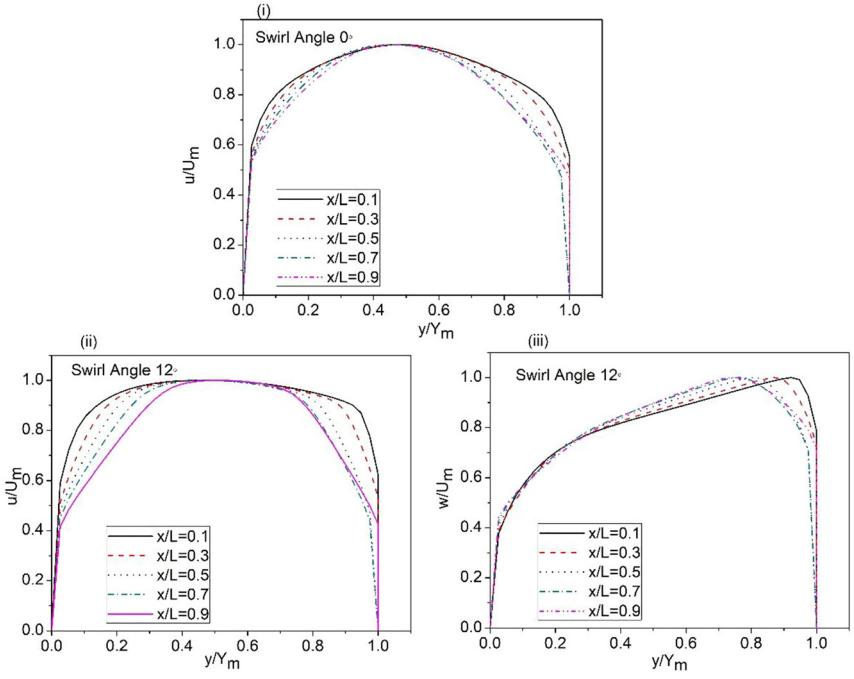

Figure 8: (i, ii) Longitudinal velocity distribution at swirl angles 0° and 12° (iii) Swirl velocity distribution at swirl angle 12°, diffuser A.

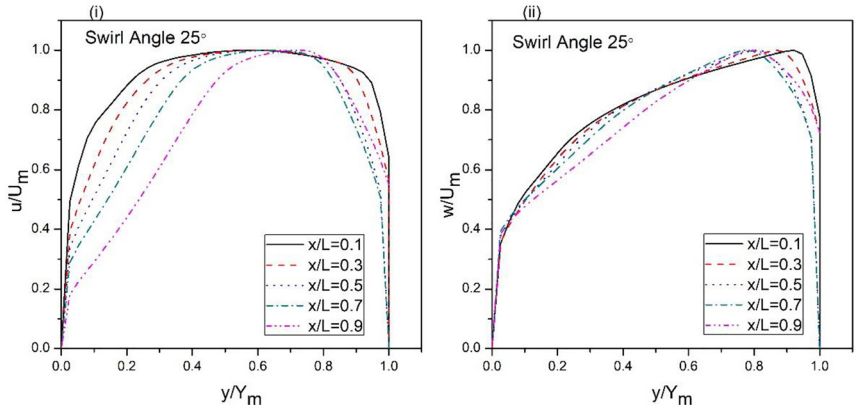

Figure 9: (i) Longitudinal velocity distribution at swirl angle 25° (ii) Swirl velocity distribution at swirl angle 25°, diffuser A.

diffuser. There is no reversal flow near the wall at the 12° inlet swirl angle. The reversal flow takes place on the hub wall for x/L = 0.3,0.5,0.7 and 0.9 at y/Y_m = 0.04,0.20,0.28 and 0.34 for the inlet swirl angle 25°. The swirl velocity profiles are shown in Figures 10(iii) and 11(ii). High swirl velocity near the casing wall caused by the forced vortexes phenomenon at swirl angles 12° and 25°.

The longitudinal velocity distribution for the C-type diffuser of AR = 3.44 and casing angle 9° are presented in Figures 12(i, ii) and 13(i). The flow reversal on the casing wall can be observed for no swirl condition. At zero degrees, the inlet swirl angle, the reverse flow takes place from y/Y_m = 0.97 and 0.92 to casing wall at x/L = 0.7 and x/L = 0.9, respectively. The separation of the flow for the inlet swirl angle 12° and above occurs on the hub wall. The separation of the flow in the C-type diffuser occurs much earlier than the B-type diffuser as the centrifugal forces push the flow towards the casing wall and there is more diffusion passage due to wide annular passage. The swirl velocity distributions plotted in Figures 12(iii) and 13(ii) depict the same nature as the earlier case due to the forced vortex nature.

Static pressure recovery coefficient (C_p)

The recovery of pressure coefficient at the casing wall of diffusers A, B, and C of ARs 1.64, 2.48, and 3.44 respectively for different inlet swirl angles along the length of non-dimensional diffuser passage (x/L) are shown in Figures 14(i), 15(i), and i16(i). For A-type diffuser, the recovery of the pressure coefficient increases continuously ahead of the diffuser passage from the non-swirling flow to the swirl flow. For a 25° inlet swirl angle, Cp is highest at the cross-section equal to x/L = 0.88. The pressure recovery rises with a swirl flow as compared to non-swirl flow at the

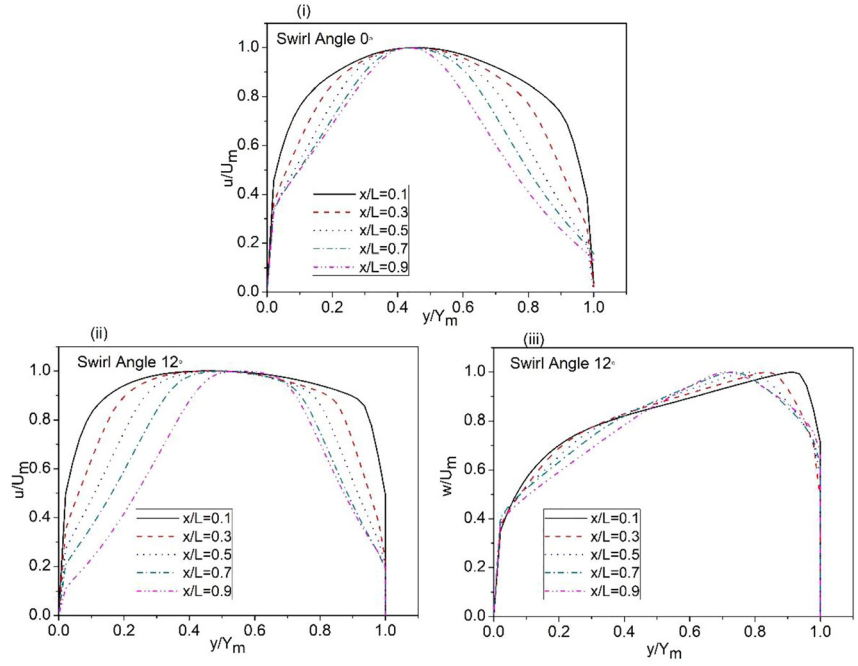

Figure 10: (i, ii) Longitudinal velocity distribution at swirl angles 0° and 12° (iii) Swirl velocity distribution at swirl angle 12°, diffuser B.

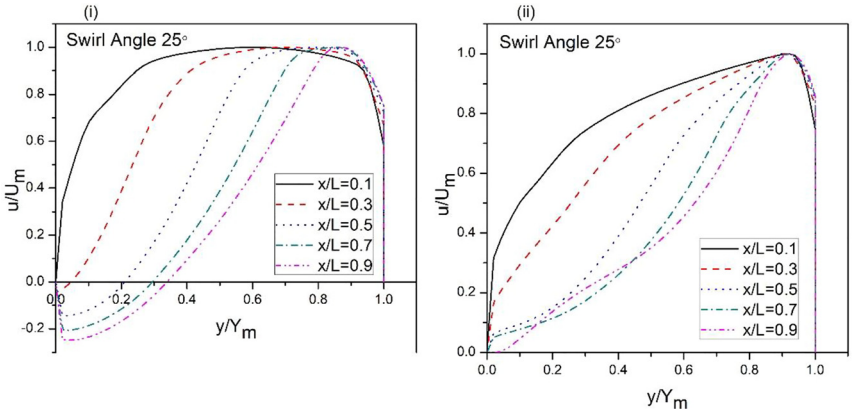

Figure 11: (i) Longitudinal velocity distribution at swirl angle 25° (ii) Swirl velocity distribution at swirl angle 25°, diffuser B.

beginning of the B-type diffuser. The maximum pressure recovery is observed on the 12°swirl angle and minimum loss coefficient in the B-type diffuser. There is a lower pressure recovery of the diffuser passage length beyond x/L = 0.50 and x/L = 0.25 at the swirl angles 17° and 25°. The reason is that the flow separation on the hub, is seen in longitudinal velocity distribution. In a C-type diffuser the magnitude of Cp of the swirl flow is lower than the 0° swirl curve at x/L = 0.56,0.48,0.15,0.12 at the different swirl angles i.e., 7.5°, 12°, 17°, and 25°. The marginal Cp increases with the swirling flow at the beginning of the diffuser passage and then decreases because of the high divergence angle of the casing; flow separation occurs on the hub and the casing wall for the swirling flow.

The C_P varies with AR and Cp for the dimensionless length for the non-swirling flow as shown in Figure 17(i, ii) respectively. The obtained simulation result shows the meticulous agreement with the outcomes of Sovran and Klomp [6]; Coladipietro et al. [10] for the three tested diffusers (A, B, C). The diffuser B produces the highest-pressure recovery in comparison to the other two type diffusers, as reflected by the curves in Figure 17(i, ii). The pressure recovery (C_p) in the A-type diffuser amongst others is very low due to the limited AR of 1.67. It has been found that 55%of pressure recovery is achieved in the C-type diffuser along the non-dimensional length. In C-type diffuser, having maximum pressure recovery up to the mid-length of the diffuser and after that pressure

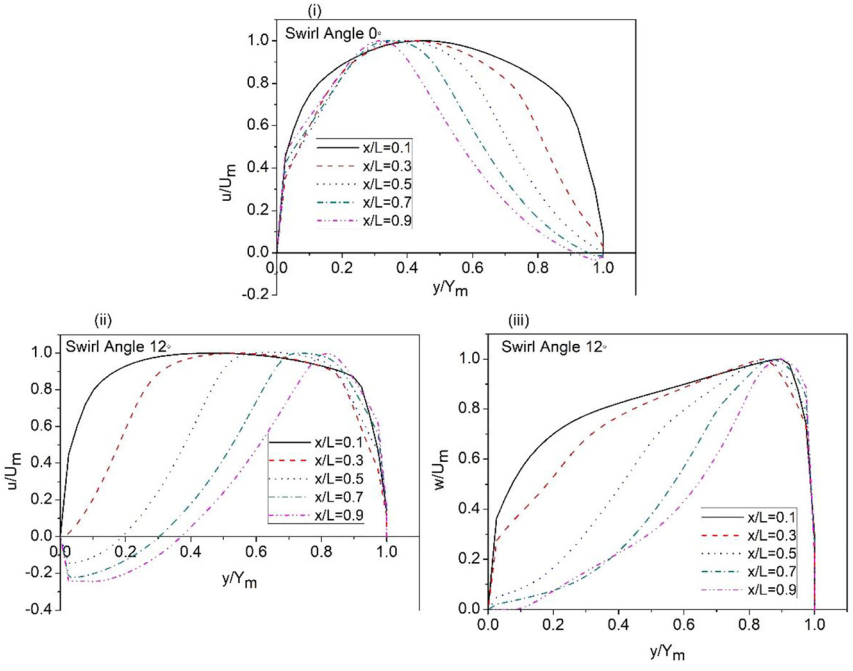

Figure 12: (i, ii) Longitudinal velocity distribution at swirl angles 0° and 12° (iii) Swirl velocity distribution at swirl angle 12°, diffuser C.

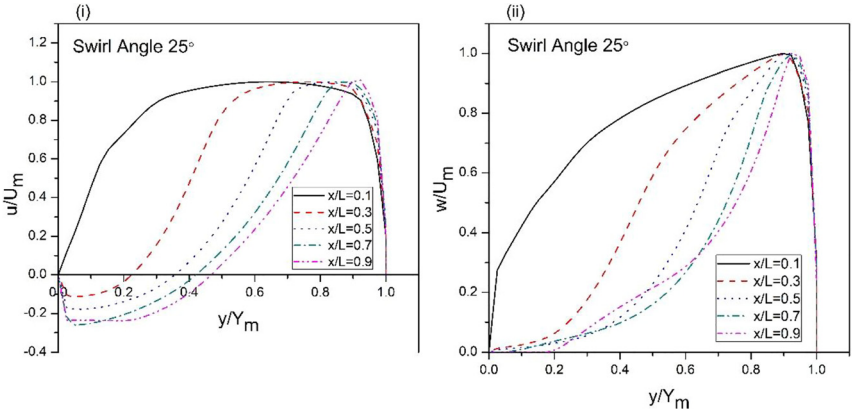

Figure 13: (i) Longitudinal velocity distribution at swirl angle 25° (ii) Swirl velocity distribution at swirl angle 25°, diffuser C.

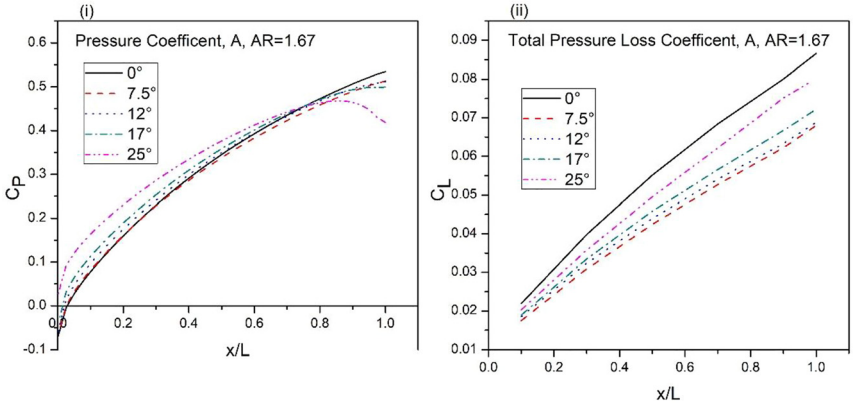

Figure 14: (i) Static pressure recovery coefficient (C_p) at casing (ii) Total pressure loss coefficient (C_{TL}), diffuser A.

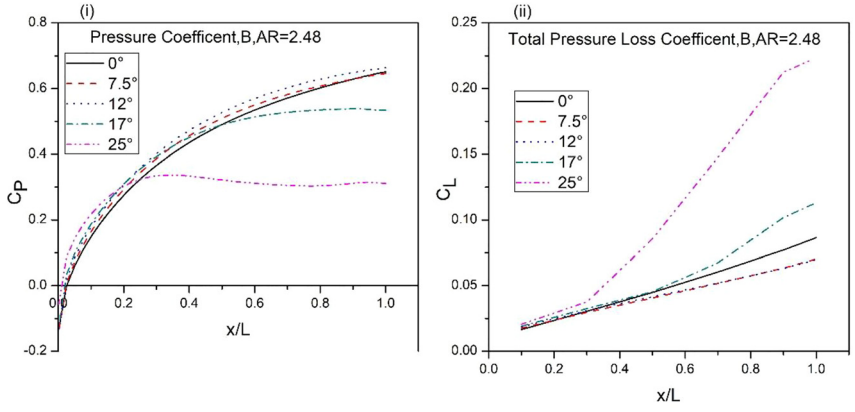

Figure 15: (i) Static pressure recovery coefficient (C_p) at casing (ii) Total pressure loss coefficient (C_{TL}), diffuser B

recovery is falling between A and B-types diffusers due to separation of flow along the wall, as shown in Figure 17(ii).

Total pressure loss coefficient

The C_{TL} of diffusers A, B, and C for AR 1.67, 2.48, and 3.67 are shown in Figures 14(ii), 15(ii), and ii16(ii).The minimum C_{TL} is observed in swirl angle 7.5° in comparison to non-swirling flow and swirl flow in A- type diffuser. It is observed that there is no separation of fluid flow on the hub wall and casing wall. The maximum loss coefficient is equal to 40% and 23% at swirl angle of 25° in B and C-type diffusers, respectively, due to the separation of fluid flow on the casing wall.

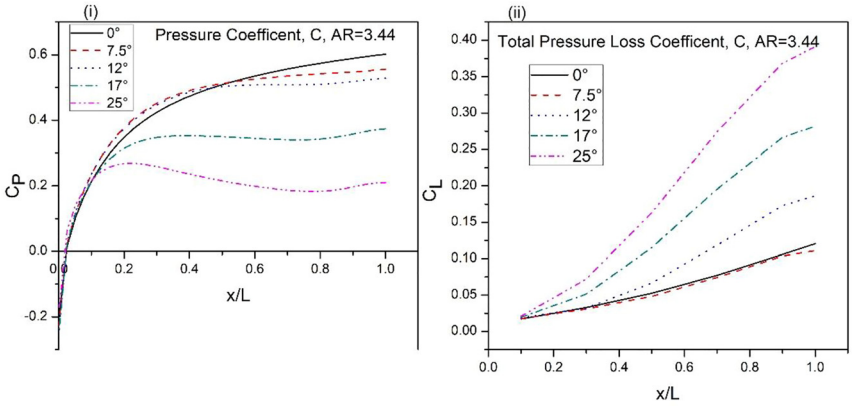

Figure 16: (i) Static pressure recovery coefficient (C_p) at casing (ii) Total pressure loss coefficient (C_{TL}), diffuser C

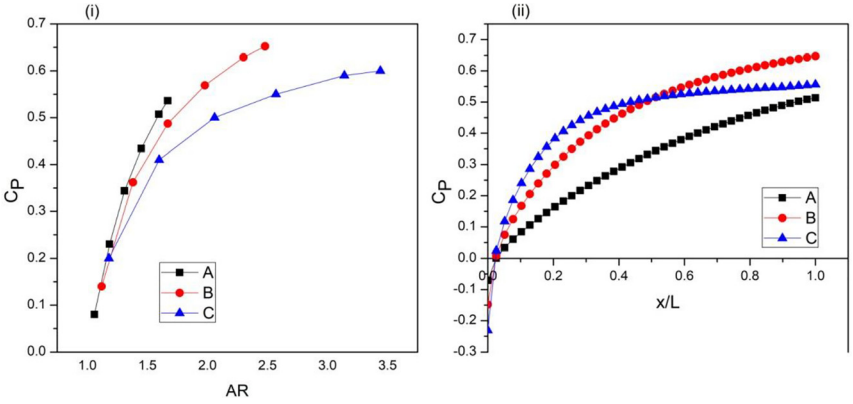

Figure 17: (i) C_p with an area ratio of diffusers A, B, and C (ii) C_p with the non-dimensional length of diffusers A, B, and C.

Conclusion

The study of non-swirling and swirling flow of straight hub axial annular diffuser has been investigated and the following results were obtained.

1. In the case of swirling flow, the longitudinal velocity distribution profile shows an increment in the local velocity continuously downstream of the diffusers.
2. With the introduction of swirl flow, the fluid flow moves towards the casing wall due to which no stall is present on the casing wall.
3. Swirls improve the pressure recovery up to a certain length, however, after that it deteriorates the performance due to the flow separation from the hub wall.
4. The maximum pressure recovery coefficient and the minimum C_{TL} are achieved in the B-type diffuser at the inlet swirl angle equal to 12°.

Author contribution: All the authors have accepted responsibility for the entire content of this submitted manuscript and approved submission.
Research funding: None declared.
Conflict of interest statement: The authors declare no conflicts of interest regarding this article.

References

1. Arora BB. Performance analysis of parallel hub diverging casing axial annular diffuser with 20 equivalent cone angle. Aust J Mech Eng 2014;12:179–94.
2. Arora BB, Pathak BD. Effect of geometry on the performance of annular diffuser. Int J Appl Eng Res 2009;5:3419–28.
3. Singh H, Arora BB. Effect of area ratio on flow separation in annular diffuser. In: Advances in fluid and thermal engineering. Singapore: Springer; 2019:297–305 pp.
4. Johnston IH. The effect of inlet conditions on the flow in annular diffusers. No. NGTE-M. 167. United Kingdom: National Gas Turbine Establishment Farnborough; 1953.
5. Reneau LR, Johnston JP, Kline SJ. Performance and design of straight, two-dimensional diffusers. J Basic Eng 1967;89:141–50.
6. Sovran G, Klomp ED. Experimentally determined optimum geometries for rectlinear diffusers with rectangular, conical or annular cross section. Fluid Mech Intern Flow 1967: 270–319.
7. Stevens SJ. Paper 16: the performance of annular diffusers. In: Proceedings of the Institution of Mechanical Engineers, Conference Proceedings Sage UK. London, England: SAGE Publications; 1967; 182; 58–70.
8. Adenubi SO. Performance and flow regime of annular diffusers with axial turbomachine discharge inlet conditions. J Fluid Eng 1976;98:236–42.
9. Stevens SJ, Fry P. Measurements of the boundary-layer growth in annular diffusers. J Aircraft 1973;10:73–80.

10. Coladipietro R, Schneider JH, Sridhar K. Effects of inlet flow conditions on the performance of equiangular annular diffusers. Trans Can Soc Mech Eng 1975;3:75–82.
11. Kumar DS, Kumar KL. Effect of swirl on pressure recovery in annular diffusers. J Mech Eng Sci 1980;22:305–13.
12. Singh SN, Agrawal DP, Sapre RN, Malhotra RC. Effect of inlet swirl on the performance of wide-angled annular diffusers. IJEMS 1994;01:63–9.
13. Singh SN, Seshadri V, Saha K, Vempati KK, Bharani S. Effect of inlet swirl on the performance of annular diffusers having the same equivalent cone angle. Proc IME G J Aero Eng 2006;220:129–43.
14. Mohan R, Singh SN, Agrawal DP. Optimum inlet swirl for annular diffuser performance using CFD. IJEMS 1998;05:15–21.
15. Ubertini S, Desideri U. Experimental performance analysis of an annular diffuser with and without struts. Exp Therm Fluid Sci 2000;22:183–95.
16. Feldcamp GK, Birk AM. Strut losses in a diverging annular diffuser with swirling flow. ASME turbo expo 2006: power for land, sea, and air. Barcelona, Spain; 2006:9-18 pp.
17. Dunn JJ, Ricklick M, Kapat JS. Flow characterization of a three-dimensional separated annular diffuser. In: ASME 2009 international mechanical engineering congress and exposition. Florida, USA: American Society of Mechanical Engineers Digital Collection; 2009:859–65 pp.
18. Buice CU, Eaton JK. Experimental investigation of flow through an asymmetric plane diffuser. In: Center for turbulence research annual research briefs; 1995:117–20 pp.
19. Ibrahim KA, Abdalla HA, El-Askary WA, Abdel-Salam AM. Numerical study on turbulent swirling flow in annular diffusers. Eng Res Bull 2007;30:551–69.
20. Kumar M, Arora BB, Maji S. Analysis of flow separation in wide angle annular diffusers. Int J Appl Eng Res 2010;5:3419–28.
21. Sadasivan S, Arumugam SK, Aggarwal MC. Numerical simulation of diffuser of a gas turbine using the actuator disc model. J Appl Fluid Mech 2019;12:77–84.
22. Hoadley D. Three-dimensional turbulent boundary layers in an annular diffuser [Ph.D. thesis]. University of Cambridge; 1970.
23. Klomp ED. Performance of straight-walled annular diffusers with swirling flow. The Aeronautical Journal 1997;101: 467–80.